NANO LETTERS

pubs.acs.org/NanoLett Letter

Nanoscale Magnetic Ordering Dynamics in a High Curie Temperature Ferromagnet

Yueh-Chun Wu, Gábor B. Halász, Joshua T. Damron, Zheng Gai, Huan Zhao, Yuxin Sun, Karin A. Dahmen, Changhee Sohn, Erica W. Carlson, Chengyun Hua, Shan Lin, Jeongkeun Song, Ho Nyung Lee, and Benjamin J. Lawrie*

Cite This: *Nano Lett.* 2025, 25, 1473–1479 Read Online

ACCESS | Metrics & More | Article Recommendations | Supporting Information

ABSTRACT: Thermally driven transitions between ferromagnetic and paramagnetic phases are characterized by critical behavior with divergent susceptibilities, long-range correlations, and spin dynamics that can span kHz to GHz scales as the material approaches the critical temperature T_c, but it has proven technically challenging to probe the relevant length and time scales with most conventional measurement techniques. In this study, we employ scanning nitrogen-vacancy center based magnetometry and relaxometry to reveal the critical behavior of a high-T_c ferromagnetic oxide near its Curie temperature. Cluster analysis of the measured temperature-dependent nanoscale magnetic textures points to a 3D universality class with a correlation length that diverges near T_c. Meanwhile, the temperature-dependent spin dynamics, measured through all optical relaxometry suggest that the phase transition is in the XY universality class. Our results capture both static and dynamic aspects of critical behavior, providing insights into universal properties that govern phase transitions in magnetic materials.

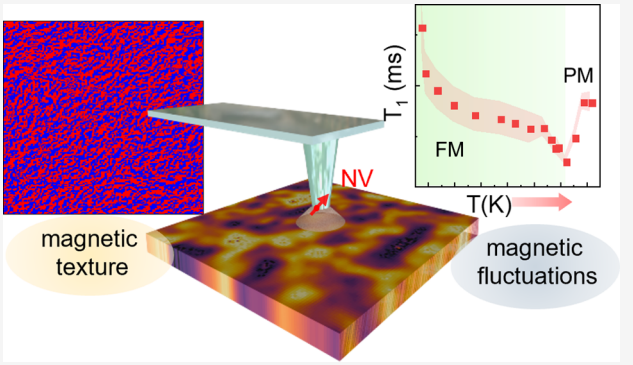

KEYWORDS: *Quantum sensing, NV center, Relaxometry*

Understanding continuous phase transitions near critical points is crucial in fundamental physics. In condensed matter physics and materials science, these transitions, often driven by variations in temperature, pressure, and external fields, reveal complex interactions among lattice structures, electronic states, and magnetic moments. Of particular interest are second-order (continuous) phase transitions, where the order parameter changes smoothly and is often associated with spontaneous symmetry breaking. Near a second-order phase transition, systems exhibit critical phenomena, including divergent correlation lengths, fluctuations, and susceptibilities. These critical phenomena fall into distinct universality classes set by, e.g., the spatial dimension and the symmetry character of the order parameter, such that scaling laws near criticality are independent of microscopic details. Understanding these behaviors provides insights into the underlying physics that governs a wide range of systems.

Over the past decade, nitrogen-vacancy (NV) centers in diamond have emerged as powerful nanoscale quantum sensors capable of probing ferromagnetic[1−3] and antiferromagnetic[4,5] ordering, and slow telegraph switching of magnetic domain walls has been observed through time-series fluorescence measurements and through variations in the measured optically detected-magnetic-resonance (ODMR) line width.[6] On the other hand, NV T_1 and T_2 measurements have increasingly been used to measure high-frequency fluctuating magnetic fields that are hard to access with conventional nanoscale magnetic probes like magnetic force microscopy.[7−18] The noninvasive visualization of magnetic textures and spin dynamics in response to changes in temperature or external fields is essential to characterizing critical phenomena associated with continuous phase transitions in magnetic systems where correlation scales diverge in time and space near the critical point. Recent studies have pointed to the potential for spin-qubit probes of critical dynamics in spin systems using spin coherence measurements,[18] but all-optical T_1 probes of critical dynamics would unlock the potential for probing materials in high-field environments where T_2 measurements are challenging to implement.

In this study, we investigate nanoscale magnetic ordering and spin fluctuations near the ferromagnetic-paramagnetic

Received: October 29, 2024
Revised: January 4, 2025
Accepted: January 7, 2025
Published: January 13, 2025

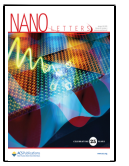

https://doi.org/10.1021/acs.nanolett.4c05401
Nano Lett. 2025, 25, 1473−1479

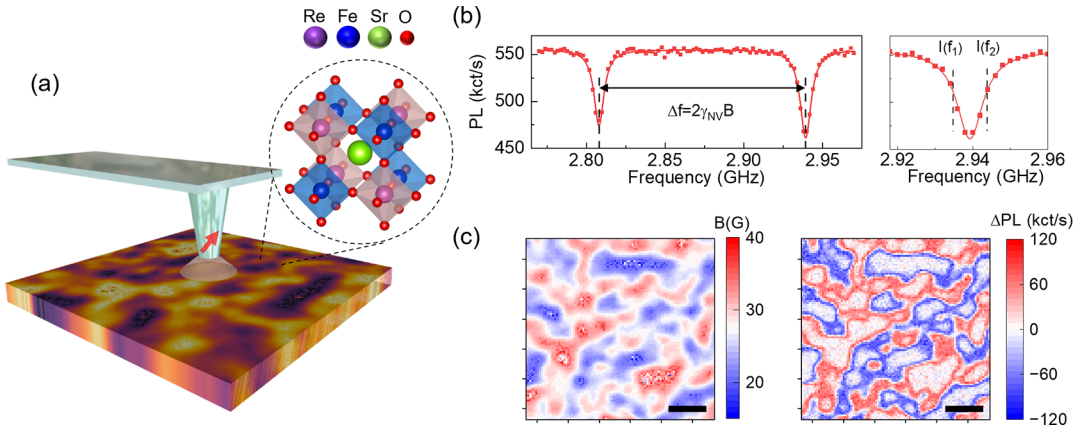

Figure 1. (a) Schematic illustration of the NV scanning microscope platform and crystal structure of the high-T_c double-perovskite ferromagnetic oxide Sr_2FeReO_6. (b) Measured ODMR spectra highlighting (left) the spectrum acquired in full-B mode to quantitatively measure the local magnetic field with no additional calibrations or assumptions and (right) the two frequencies that are used in dual-iso-B mode for high speed imaging of local magnetic textures. (c) Surface magnetic texture of Sr_2FeReO_6 measured at room temperature using (left) full-B mode and (right) dual-iso-B mode. Scale bar: 400 nm.

(FM-PM) phase transition in a thin film of the high-T_c double perovskite strontium iron rhenium oxide (Sr_2FeReO_6) using scanning NV magnetometry and relaxometry. Our results reveal the onset of magnetization characterized by surface magnetic textures that exhibit robust scaling behavior indicative of a second-order phase transition. Concurrently, we observe a pronounced increase in spin fluctuations near T_c, which are detected through NV T_1 relaxometry and modeled using Landau−Ginzburg theory. The combined results highlight the pivotal role of spin dimensionality in Sr_2FeReO_6 and more generally illustrate the importance of complementing bulk dc magnetization measurements with nanoscale probes of spin ordering and spin fluctuations, as these nanoscale energetics and dynamics ultimately drive the functionality of emerging dissipationless spin-based information processing platforms.

We focus here on the high-T_c double perovskite Sr_2FeReO_6, whose crystal structure is illustrated in Figure 1(a). Sr_2FeReO_6 is known for its robust ferromagnetism persistent up to 400 K,[19,20] and unlike most metallic ferromagnets, the ferromagnetism in Sr_2FeReO_6 is attributed to a hybridization mechanism.[21] The ferromagnetic order in Sr_2FeReO_6 is stabilized by significant exchange splitting of Fe 3d orbitals, driven by strong electron−electron correlations, and spin-dependent hybridization between Fe 3d and Re 5d orbitals. As a result, the electronic band structure of Sr_2FeReO_6 near the Fermi level is dominated by spin-polarized Re 5d orbitals, as demonstrated in previous DFT calculations.[22] This combination of half-metallic character, strong electron correlations from 3d orbitals, and large spin−orbit coupling in 5d orbitals makes Sr_2FeReO_6 not only promising for spintronic applications but also a potential platform for a quantum anomalous Hall insulator phase.[21] Here, a high quality epitaxial thin film of Sr_2FeReO_6 with thickness ∼35 nm was grown with a sintered Sr_2FeReO_6 target by pulsed laser deposition on a (001) $SrTiO_3$ substrate as previously described.[19]

Figure 1(a) illustrates the scanning NV experiment conducted here using a Qnami ProteusQ microscope, where single-NV spin states are manipulated via optical and radio frequency (RF) pulses. The NV spin is pumped into the $|0\rangle$ state by an off-resonant 520 nm optical excitation, an RF excitation with frequency around 3 GHz is used to manipulate the ground state spin, and the NV spin can be read out by measuring the NV luminescence intensity, which is larger for the $|0\rangle$ state than the Zeeman-split $|\pm 1\rangle$ states.[23] The probe used here incorporates a single negatively charged NV center implanted ∼10 nm below the surface of a (100) diamond nanopillar integrated into a tuning-fork AFM probe. The NV center axis is orientated at an angle of about 55° relative to the surface normal and is thus sensitive to changes in both in-plane and out-of-plane fields.

This approach enables nanoscale resolution, achieving detail down to 50 nm, by mapping surface magnetic textures through ODMR measurements taken at each pixel of the image. In full-B mode, the magnetic field is calculated from the frequency separation between the $|\pm 1\rangle$ states observed in the ODMR spectrum, as shown in the left of Figure 1(c) via the relationship $B_z = \frac{\Delta\nu}{2\gamma}$ where $\Delta\nu$ represents the frequency separation and γ = 28 GHz/T is the electron gyromagnetic ratio. However, acquiring a full ODMR spectrum at each pixel of an image can be time-consuming; the dual-iso-B measurement protocol provides an alternative high-speed measurement modality in which a single ODMR spectrum is acquired in order to define the frequencies f_1 and f_2 illustrated in the right of Figure 1(c) at the full-width half-maximum of a $|0\rangle$ to $|\pm 1\rangle$ transition. The luminescence intensity is then measured at each pixel of the image for RF excitation at f_1 and f_2. For small changes in magnetic field, the differential photoluminescence intensity $\Delta PL = PL(f_1) - PL(f_2)$ can be mapped to changes in the magnetic field semiquantitatively.

Figure 1(d) displays the nanoscale magnetic surface texture of a ferromagnetic Sr_2FeReO_6 thin film measured in full-B mode (left) and dual-iso-B mode (right). The resolved magnetic domains exhibit structure across measured length scales spanning ∼50 nm to 15 μm (with a 2 μm illustrated field of view in Figure 1(d)),and the measured magnetic field varies by 10−15 G across the full-B map. This dynamic range is sufficiently small to allow for accurate high-speed measurements to be acquired in dual-iso-B mode, as is seen in the qualitative one-to-one relationship between the full-B and dual-iso-B maps in Figure 1(d).

The nanoscale resolution of magnetic textures under external stimuli, such as magnetic field and temperature,

https://doi.org/10.1021/acs.nanolett.4c05401
Nano Lett. 2025, 25, 1473−1479

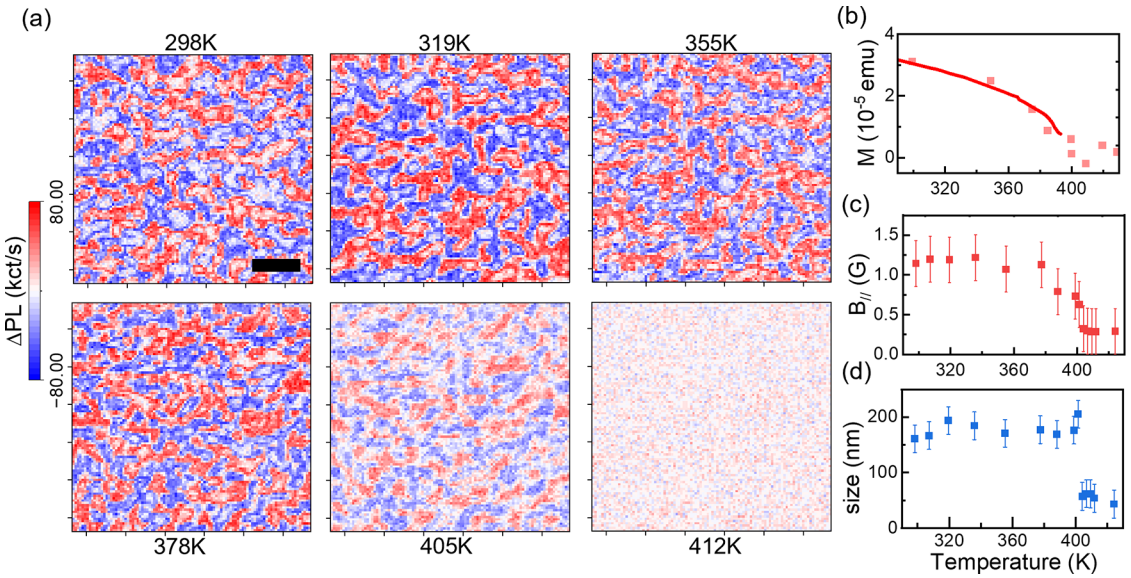

Figure 2. (a) Dual-iso-B scans acquired as a function of temperature for representative temperatures between 298 and 412 K. Scale bar: 1 μm. (b) In-plane bulk M(T) curve of Sr_2FeReO_6 measured at H = 1 kOe. Solid dots are M_S(T) data obtained using a high temperature oven to determine the T_c. Isothermal magnetization curves were measured between ±4 kOe due to sample holder size limitations. The data above ±1 kOe were linearly fit to estimate M_S(T). (c) NV sensed magnetic field strength. (d) Magnetic texture size estimated from temperature dependent NV dual-iso-B magnetometry scans. The approach used to extract the data in (c) and (d) is described in greater detail in the Supporting Information.

provides valuable insights into magnetic ordering in correlated materials that are critical to the development of dissipationless electronic and spintronic devices, as bulk magnetization measurements do not provide a complete picture of spin interactions within and between domains. In the absence of a strong magnetic field, the thermally induced FM-PM phase transition exhibits characteristics of a second-order phase transition.[24−26] We probed this transition with temperature-dependent scanning NV microscopy, which was performed in dual-iso-B mode to minimize deleterious effects from drift at elevated temperatures. In Figure 2(a), the FM-PM transition is clearly visualized between 397 and 412 K with the disappearance of any measurable long-range magnetic order. To quantify this behavior, we performed a contrast analysis by comparing the most and least intense areas (top and bottom 10% average, respectively) from the distribution in each false-color map, and we extracted the effective magnetic field strength using an inverse Lorentzian transformation linking count differences to field-induced ODMR shifts. As illustrated in Figure 2(c), the stray magnetic field strength, and the associated surface magnetization rapidly drops as the temperature approaches 400 K. We further compare the extracted magnetic field strength with bulk magnetization measurement data acquired with a superconducting quantum interference device[19] in Figure 2(b). The data in Figures 2(b) and 2(c) show excellent agreement in the onset and gradual increase of the magnetization near the phase transition.

Further analysis involved binarizing the images and performing autocorrelations to estimate the average spatial length scale of the magnetic texture (see Supporting Information). Interestingly, this analysis reveals that the average texture size remains constant (~200 nm) over a broad temperature range from 298 to 400 K [see Figure 2(d)]. We note that this magnetic texture evolution contrasts with first-order transitions driven by external fields where domains gradually grow as long-range magnetic order is established with defects and local disorder serving as nucleation sites.

The gradual onset of magnetization, coupled with the observed texture evolution, is characteristic of a second-order phase transition, where power law scaling behavior is anticipated. To evaluate this scaling in the measured magnetic domain structure, we extract the radius of gyration (R_g), a parameter that represents the average distance between two points within a given magnetic cluster. Near the phase transition, NV magnetometry scans of the ordered phase ($T < T_c$) were performed with both large (15 μm) and small (2 μm) fields of view. The bilogarithmic plot of R_g against cluster area (A) shown in Figure 3 reveals a power law scaling behavior spanning two and half decades, with the exponent d_v = 1.73 ± 0.04. Similarly, a robust power-law scaling is observed in the cluster perimeter (P) as a function of R_g, with the exponent d_h = 1.34 ± 0.04. Critical phenomena are governed by the concept of universality, where critical exponents depend

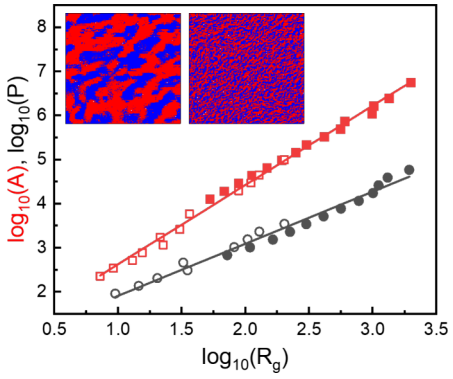

Figure 3. Scaling analysis of cluster area (A) and perimeter (P) against the gyration radius R_g from dual-iso-B maps acquired in the ordered phase ($T > T_c$). The plotted data points are derived by combining data from the maps shown in the inset that were each acquired with 200 × 200 pixel resolution across (left) 2 μm and (right) 15 μm fields of view.

https://doi.org/10.1021/acs.nanolett.4c05401
Nano Lett. 2025, 25, 1473−1479

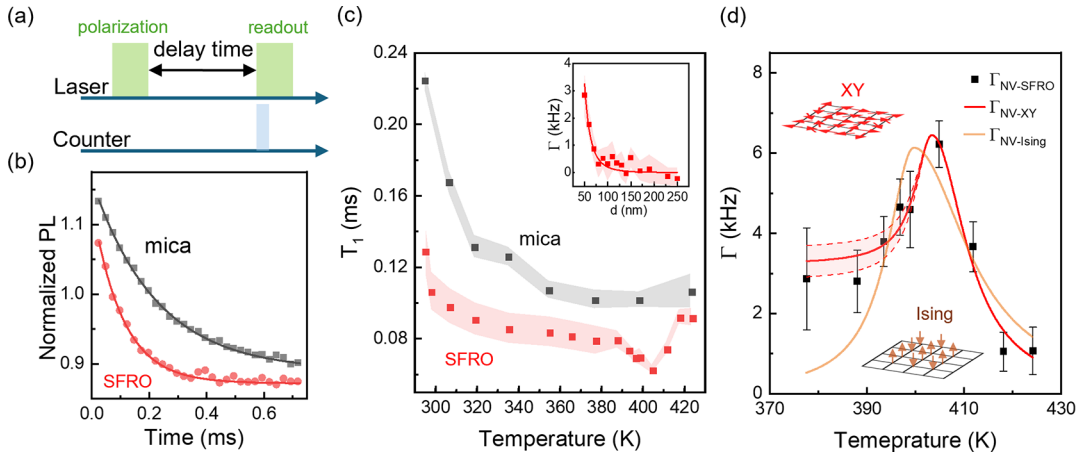

Figure 4. (a) Pulse sequence for all-optical NV T_1 relaxometry. (b) NV T_1 relaxation when a single NV is brought into proximity of Sr_2FeReO_6 (red) and mica (black). (c) Temperature dependent T_1 spin relaxation time of a NV center interacting with Sr_2FeReO_6 (red) and mica (black). The uncertainty (shaded area) is calculated based on a procedure described in the Supporting Information. Inset: Height-dependent relaxation rate Γ is calculated as $\Gamma_{SFRO} - \Gamma_{mica}$ at 405 K and fitted to the functional form $\frac{1}{d^3} - \frac{1}{(d+D)^3}$. (d) NV relaxation rate (Γ) near the FM-PM second order phase transition. The experimental data (black dots) are fitted with Landau−Ginzburg theories assuming XY and Ising universality classes. In the XY case, the solid line corresponds to an in-plane NV rotation angle of $\theta = 45°$, with the shaded region representing the possible range of θ between 0° and 90° (see Supporting Information for details).

on dimensionality and symmetry rather than material-specific details. In our result where SFRO is probed near the critical point (T_c), these critical exponents suggest a three-dimensional universality class for the spin system (see Supporting Information). Characterizing critical exponents is crucial and our results highlight the power of NV magnetometry in understanding critical phenomena in second-order magnetic phase transitions.

On the other hand, magnetic fluctuations, which reflect dynamical deviations from spin equilibrium, can provide a complementary understanding of critical phenomena near continuous phase transitions. Measurements of the NV spin relaxation lifetime T_1 and coherence time T_2 have increasingly emerged as sensitive quantum probes of magnetic noise in an extensive frequency range.[13,27−29] In particular, the change in T_1 relative to the intrinsic T_1 for an NV center interacting with a fluctuating spin system via dipole−dipole interactions is proportional to the dynamical spin structure factor at the intrinsic NV frequency corresponding to the level splitting.

In the all-optical T_1 relaxometry sensing protocol used here, the NV spin state is initially polarized to $m_s = 0$ by an optical pulse. The relaxation process is then monitored by a second optical pulse reading out the luminescence intensity as a function of delay time, as depicted in Figure 4(a). The initialization and read-out laser pulses each have a duration of 5 μs, while the counting windows for both the reference and signal are 300 ns. A similar NV T_1 relaxometry technique has recently been demonstrated to capture the increased magnetic noise near a magnetic phase transition in 2D α-Fe_2O_3.[30] In that context, the increase in magnetic fluctuations inferred from the T_1 relaxation is relevant to the in-plane/out-of-plane switching of antiferromagnetic ordering. To study magnetic ordering and the FM-PM continuous phase transition, we first compare T_1 relaxation times for the NV tip brought into proximity with Sr_2FeReO_6 and mica (respectively) for two reasons. First, the spin relaxation time of NV centers can vary under different tip conditions, as NV centers are known to be sensitive to surface condition and nearby impurities.[27,31] Second, in diamagnetic systems like mica, the magnetic dipole−dipole interaction is absent due to the diminished net magnetic moment of paired electrons. Therefore, the NV T_1 on mica serves as a reference for the intrinsic temperature-dependent NV spin dynamics. Representative T_1 measurements acquired at 300 K on mica and Sr_2FeReO_6 are shown in Figure 4(b), and the temperature-dependent spin lifetime is shown in Figure 4(c).

Below T_c, the NV center T_1 is suppressed for ferromagnetic Sr_2FeReO_6 compared to the baseline temperature-dependent NV T_1 acquired on mica as a result of magnetic noise generated by the ferromagnetic spin bath. According to the fluctuation−dissipation theorem, the magnetic noise of a system is related to the imaginary part of the dynamical magnetic susceptibility.[23,30,32] At temperatures approaching T_c = 405 K, Figure 4(c) highlights the additional increase in the NV center spin relaxation rate compared with the intrinsic spin dynamics measured on the mica substrate, which can be understood as a direct result of the magnetic susceptibility diverging near a second order phase transition.[24,25,33] Near T_c, the system is in a state of critical instability where the spins become increasingly correlated over large distances.[26,34] This increased spin−spin correlation leads to enhanced fluctuations as the spins spontaneously align with perturbing fields. NV relaxometry, given its susceptibility to magnetic fluctuations, is therefore a powerful tool for the characterization of continuous magnetic phase transitions.

To provide a more quantitative understanding, we apply a mean-field Landau−Ginzburg theory, which effectively captures the magnetic fluctuations near T_c. This theory incorporates the interaction between a NV center and a spin bath based on different spin models. As described in greater detail in the Supporting Information, we treat Sr_2FeReO_6 as an infinite slab of thickness D with magnetic fluctuations measured by a NV center at distance d above its surface. For the Ising universality class, the NV relaxation rate takes the general form

$$\frac{1}{T_1} \propto T\left[\frac{1}{d^3} - \frac{1}{(d+D)^3}\right]\frac{16}{\alpha^2 \max(\tau, -2\tau)^2 + \gamma^2\omega_0^2} \quad (1)$$

https://doi.org/10.1021/acs.nanolett.4c05401
Nano Lett. 2025, 25, 1473−1479

where $\tau = T - T_c$ is the relative temperature, ω_0 is the intrinsic frequency of the NV center, γ is a damping coefficient, and α is an unknown Landau parameter. In the XY universality class, the same relaxation rate becomes

$$\frac{1}{T_1} \propto T\left[\frac{1}{d^3} - \frac{1}{(d+D)^3}\right]\left\{\frac{7 + 2\sin^2\theta}{\alpha^2 \max(\tau, -2\tau)^2 + \gamma^2\omega_0^2} + \frac{7 + 2\cos^2\theta}{\alpha^2 \max(\tau, 0)^2 + \gamma^2\omega_0^2}\right\} \quad (2)$$

where θ is an in-plane rotation angle between the NV direction and the given ferromagnetic domain. (Note that the relaxation rate in eq 2 becomes independent of θ in the paramagnetic phase, $\tau > 0$, as expected.) Unlike in the Ising universality class, the NV relaxation rate in the XY universality class remains finite in the ferromagnetic phase even for large relative temperatures, $|\tau| \gg \gamma\omega_0/\alpha$, which is consistent with the measured temperature-dependent spin dynamics plotted in Figure 4(d). Indeed, while the height-dependent spin relaxation rate plotted in the inset of Figure 4(c) is consistent with both Ising and XY universality classes due to the same $\frac{1}{d^3} - \frac{1}{(d+D)^3}$ scaling, the temperature-dependent behavior in the ferromagnetic phase [see Figure 4(d)] points to the XY universality class.

To further examine the magnetic texture dependent T_1, we conducted an iso-T_1 scan where the decay in fluorescence intensity is monitored at a given delay time as a function of NV center position (see Supporting Information). The T_1 time for an NV center interacting with local magnetic textures can be estimated assuming a single exponential decay behavior across the scanning area. One might naively expect T_1 to vary with the spatially varying magnetic texture as a result of reduced cross-relaxation[35,36] as the magnetic field lifts the spin degeneracy. However, no statistically significant correspondence was found between T_1 and the mapped magnetic texture. This discrepancy may arise from the complex magnetic structure of Sr_2FeReO_6, which exhibits magnetic anisotropy between in-plane and out-of-plane directions, as indicated by bulk magnetization measurements (see Supporting Information). This complexity hinders a straightforward correlation between stray field profiles and magnetic domain morphology, thus complicating the comparison of spin noise contributions from domain walls and domains. Spatially resolved T_1 measurements were also examined at elevated temperatures, including $T \sim T_c$, where the iso-T_1 maps showed no apparent spatial dependence on weak magnetic textures.

In conclusion, we have studied the continuous phase transition of the high-T_c ferromagnetic oxide Sr_2FeReO_6 using scanning NV magnetometry and relaxometry, which provide quantitative, minimally perturbative probes of spin ordering and spin dynamics. The power-law scaling behavior observed in the magnetic texture is a powerful way of understanding the phase transition and suggests that the critical point is in a 3D universality class. With the magnetic fluctuations complementarily sensed by NV relaxometry across the phase transition, we can then argue that the ferromagnetic Sr_2FeReO_6 thin film can be modeled as a 3D XY spin system on length scales comparable to the film thickness. We note that a dimensional crossover might happen if the film thickness is further reduced to the length scale of the spin−spin interactions. The nature of the phase transition in this scenario would pose an interesting question as there is no long-range magnetic order for spin systems with continuous symmetries in the 2D limit.

■ ASSOCIATED CONTENT

Supporting Information

The Supporting Information is available free of charge at https://pubs.acs.org/doi/10.1021/acs.nanolett.4c05401.

Image analysis, magnetization analysis, cluster analysis, modeling of magnetic fluctuations, spatially resolved spin-lifetime measurements, and universality class analysis. (PDF)

■ AUTHOR INFORMATION

Corresponding Author

Benjamin J. Lawrie − *Materials Science and Technology Division, Oak Ridge National Laboratory, Oak Ridge, Tennessee 37831, United States;* orcid.org/0000-0003-1431-066X; Email: lawriebj@ornl.gov

Authors

Yueh-Chun Wu − *Materials Science and Technology Division, Oak Ridge National Laboratory, Oak Ridge, Tennessee 37831, United States*

Gábor B. Halász − *Materials Science and Technology Division, Oak Ridge National Laboratory, Oak Ridge, Tennessee 37831, United States*

Joshua T. Damron − *Chemical Sciences Division, Oak Ridge National Laboratory, Oak Ridge, Tennessee 37831, United States;* orcid.org/0000-0003-3409-0190

Zheng Gai − *Center for Nanophase Materials Sciences, Oak Ridge National Laboratory, Oak Ridge, Tennessee 37831, United States;* orcid.org/0000-0002-6099-4559

Huan Zhao − *Center for Nanophase Materials Sciences, Oak Ridge National Laboratory, Oak Ridge, Tennessee 37831, United States;* orcid.org/0000-0002-4982-0865

Yuxin Sun − *Department of Physics, Purdue University, West Lafayette, Indiana 47907, United States; Purdue Quantum Science and Engineering Institute, West Lafayette, Indiana 47907, United States;* orcid.org/0000-0001-6024-7601

Karin A. Dahmen − *Department of Physics, University of Illinois, Urbana−Champaign, Illinois 61801, United States*

Changhee Sohn − *Materials Science and Technology Division, Oak Ridge National Laboratory, Oak Ridge, Tennessee 37831, United States; Department of Physics, Ulsan National Institute of Science and Technology, Ulsan 44919, South Korea;* orcid.org/0000-0002-5043-497X

Erica W. Carlson − *Department of Physics, Purdue University, West Lafayette, Indiana 47907, United States; Purdue Quantum Science and Engineering Institute, West Lafayette, Indiana 47907, United States*

Chengyun Hua − *Materials Science and Technology Division, Oak Ridge National Laboratory, Oak Ridge, Tennessee 37831, United States*

Shan Lin − *Materials Science and Technology Division, Oak Ridge National Laboratory, Oak Ridge, Tennessee 37831, United States;* orcid.org/0000-0001-8898-6481

Jeongkeun Song − *Materials Science and Technology Division, Oak Ridge National Laboratory, Oak Ridge, Tennessee 37831, United States*

https://doi.org/10.1021/acs.nanolett.4c05401
Nano Lett. 2025, 25, 1473−1479

Ho Nyung Lee − *Materials Science and Technology Division, Oak Ridge National Laboratory, Oak Ridge, Tennessee 37831, United States;* orcid.org/0000-0002-2180-3975

Complete contact information is available at: https://pubs.acs.org/10.1021/acs.nanolett.4c05401

Notes

The authors declare no competing financial interest.

■ ACKNOWLEDGMENTS

This research was sponsored by the U.S. Department of Energy, Office of Science, Basic Energy Sciences, Materials Sciences and Engineering Division and in part by the Computational Materials Sciences Program and Center for Predictive Simulation of Functional Materials. Scanning NV microscopy was supported by the Center for Nanophase Materials Sciences (CNMS), which is a US Department of Energy, Office of Science User Facility at Oak Ridge National Laboratory. YS and EC acknowledge support from from the Department of Energy under grant DOE-QIS (DE-FOA-0002449). EC acknowledges support from NSF Grant no. DMR-2006192. KD thanks the University of Illinois at Urbana−Champaign for support. This manuscript has been authored by UT-Battelle, LLC, under contract DE-AC05-00OR22725 with the US Department of Energy (DOE). The US government retains and the publisher, by accepting the article for publication, acknowledges that the US government retains a nonexclusive, paid-up, irrevocable, worldwide license to publish or reproduce the published form of this manuscript, or allow others to do so, for US government purposes. DOE will provide public access to these results of federally sponsored research in accordance with the DOE Public Access Plan (http://energy.gov/downloads/doe-public-access-plan).

■ REFERENCES

(1) Žaper, L.; Rickhaus, P.; Wyss, M.; Gross, B.; Wagner, K.; Poggio, M.; Braakman, F. Scanning Nitrogen-Vacancy Magnetometry of Focused-Electron-Beam-Deposited Cobalt Nanomagnets. *ACS Applied Nano Materials* **2024**, *7*, 3854−3860.

(2) Celano, U.; Zhong, H.; Ciubotaru, F.; Stoleriu, L.; Stark, A.; Rickhaus, P.; de Oliveira, F. F.; Munsch, M.; Favia, P.; Korytov, M.; et al. Probing magnetic defects in ultra-scaled nanowires with optically detected spin resonance in nitrogen-vacancy center in diamond. *Nano Lett.* **2021**, *21*, 10409−10415.

(3) Sun, Q.-C.; Song, T.; Anderson, E.; Brunner, A.; Förster, J.; Shalomayeva, T.; Taniguchi, T.; Watanabe, K.; Gräfe, J.; Stöhr, R.; et al. Magnetic domains and domain wall pinning in atomically thin $CrBr_3$ revealed by nanoscale imaging. *Nat. Commun.* **2021**, *12*, 1989.

(4) Meisenheimer, P.; Moore, G.; Zhou, S.; Zhang, H.; Huang, X.; Husain, S.; Chen, X.; Martin, L. W.; Persson, K. A.; Griffin, S.; et al. Switching the spin cycloid in BiFeO3 with an electric field. *Nat. Commun.* **2024**, *15*, 2903.

(5) Ding, Z.; Sun, Y.; Zheng, N.; Ma, X.; Wang, M.; Zang, Y.; Yu, P.; Chen, Z.; Wang, P.; Wang, Y.; et al. Observation of uniaxial strain tuned spin cycloid in a freestanding BiFeO3 film. *Adv. Funct. Mater.* **2023**, *33*, 2213725.

(6) Jenkins, A.; Pelliccione, M.; Yu, G.; Ma, X.; Li, X.; Wang, K. L.; Jayich, A. C. B. Single-spin sensing of domain-wall structure and dynamics in a thin-film skyrmion host. *Physical Review Materials* **2019**, *3*, 083801.

(7) Schäfer-Nolte, E.; Schlipf, L.; Ternes, M.; Reinhard, F.; Kern, K.; Wrachtrup, J. Tracking temperature-dependent relaxation times of ferritin nanomagnets with a wideband quantum spectrometer. *Phys. Rev. Lett.* **2014**, *113*, 217204.

(8) McCullian, B. A.; Thabt, A. M.; Gray, B. A.; Melendez, A. L.; Wolf, M. S.; Safonov, V. L.; Pelekhov, D. V.; Bhallamudi, V. P.; Page, M. R.; Hammel, P. C. Broadband multi-magnon relaxometry using a quantum spin sensor for high frequency ferromagnetic dynamics sensing. *Nat. Commun.* **2020**, *11*, 5229.

(9) Du, C.; Van der Sar, T.; Zhou, T. X.; Upadhyaya, P.; Casola, F.; Zhang, H.; Onbasli, M. C.; Ross, C. A.; Walsworth, R. L.; Tserkovnyak, Y.; et al. Control and local measurement of the spin chemical potential in a magnetic insulator. *Science* **2017**, *357*, 195−198.

(10) Finco, A.; Haykal, A.; Tanos, R.; Fabre, F.; Chouaieb, S.; Akhtar, W.; Robert-Philip, I.; Legrand, W.; Ajejas, F.; Bouzehouane, K.; et al. Imaging non-collinear antiferromagnetic textures via single spin relaxometry. *Nat. Commun.* **2021**, *12*, 767.

(11) Kolkowitz, S.; Safira, A.; High, A.; Devlin, R.; Choi, S.; Unterreithmeier, Q.; Patterson, D.; Zibrov, A.; Manucharyan, V.; Park, H.; et al. Probing Johnson noise and ballistic transport in normal metals with a single-spin qubit. *Science* **2015**, *347*, 1129−1132.

(12) Andersen, T. I.; Dwyer, B. L.; Sanchez-Yamagishi, J. D.; Rodriguez-Nieva, J. F.; Agarwal, K.; Watanabe, K.; Taniguchi, T.; Demler, E. A.; Kim, P.; Park, H.; et al. Electron-phonon instability in graphene revealed by global and local noise probes. *Science* **2019**, *364*, 154−157.

(13) McLaughlin, N. J.; Hu, C.; Huang, M.; Zhang, S.; Lu, H.; Yan, G. Q.; Wang, H.; Tserkovnyak, Y.; Ni, N.; Du, C. R. Quantum imaging of magnetic phase transitions and spin fluctuations in intrinsic magnetic topological nanoflakes. *Nano Lett.* **2022**, *22*, 5810−5817.

(14) Pelliccione, M.; Myers, B. A.; Pascal, L. M. A.; Das, A.; Bleszynski Jayich, A. C. Two-dimensional nanoscale imaging of gadolinium spins via scanning probe relaxometry with a single spin in diamond. *Physical Review Applied* **2014**, *2*, 054014.

(15) Schmid-Lorch, D.; Häberle, T.; Reinhard, F.; Zappe, A.; Slota, M.; Bogani, L.; Finkler, A.; Wrachtrup, J. Relaxometry and dephasing imaging of superparamagnetic magnetite nanoparticles using a single qubit. *Nano Lett.* **2015**, *15*, 4942−4947.

(16) Tetienne, J.-P.; Lombard, A.; Simpson, D. A.; Ritchie, C.; Lu, J.; Mulvaney, P.; Hollenberg, L. C. Scanning nanospin ensemble microscope for nanoscale magnetic and thermal imaging. *Nano Lett.* **2016**, *16*, 326−333.

(17) McCullian, B. A. *Detection of Ferromagnetic Dynamics Using NV Centers in Diamond*; The Ohio State University, 2020.

(18) Ziffer, M. E.; Machado, F.; Ursprung, B.; Lozovoi, A.; Tazi, A. B.; Yuan, Z.; Ziebel, M. E.; Delord, T.; Zeng, N.; Telford, E.; et al. Quantum Noise Spectroscopy of Critical Slowing Down in an Atomically Thin Magnet. *arXiv preprint* **2024**, 2407.05614.

(19) Sohn, C.; Skoropata, E.; Choi, Y.; Gao, X.; Rastogi, A.; Huon, A.; McGuire, M. A.; Nuckols, L.; Zhang, Y.; Freeland, J. W.; et al. Room-Temperature Ferromagnetic Insulating State in Cation-Ordered Double-Perovskite $Sr_2Fe_{1+x}Re_{1-x}O_6$ Films. *Adv. Mater.* **2019**, *31*, 1805389.

(20) Zhang, Z.; Yan, H.; Huang, Z.; Chi, X.; Li, C.; Lim, Z. S.; Zeng, S.; Han, K.; Omar, G. J.; Jin, K.; et al. Tunable Magnetic Properties in Sr2FeReO6 Double-Perovskite. *Nano Lett.* **2022**, *22*, 9900−9906.

(21) Baidya, S.; Waghmare, U. V.; Paramekanti, A.; Saha-Dasgupta, T. High-temperature large-gap quantum anomalous Hall insulating state in ultrathin double perovskite films. *Phys. Rev. B* **2016**, *94*, 155405.

(22) Choi, S.-Y.; Noh, G.; Lee, H.; Kim, Y.-J.; Jin, Y.; Lee, D.; Lee, H. N.; Lee, J.; Yang, C.-H.; Sohn, C. Spin−Orbit-Lattice Locking in Strain-Engineered Sr2FeReO6 Double Perovskites. www.researchsquare.com/article/rs-3373483/v1, 2023.

(23) Casola, F.; Van Der Sar, T.; Yacoby, A. Probing condensed matter physics with magnetometry based on nitrogen-vacancy centres in diamond. *Nature Reviews Materials* **2018**, *3*, 1−13.

(24) *Statistical Physics: An Introduction*; Springer Berlin Heidelberg: Berlin, Heidelberg, 2007; pp 133−145.

(25) Zinn-Justin, J. *Phase transitions and renormalization group*; Oxford University Press, 2007.

(26) Nishimori, H.; Ortiz, G. *Elements of phase transitions and critical phenomena*; Oxford University Press, 2011.
(27) Kumar, J.; Yudilevich, D.; Smooha, A.; Zohar, I.; Pariari, A. K.; Stöhr, R.; Denisenko, A.; Hücker, M.; Finkler, A. Room Temperature Relaxometry of Single Nitrogen Vacancy Centers in Proximity to α-RuCl3 Nanoflakes. *Nano Lett.* **2024**, *24*, 4793−4800.
(28) Rollo, M.; Finco, A.; Tanos, R.; Fabre, F.; Devolder, T.; Robert-Philip, I.; Jacques, V. Quantitative study of the response of a single NV defect in diamond to magnetic noise. *Phys. Rev. B* **2021**, *103*, 235418.
(29) Lamichhane, S.; Timalsina, R.; Schultz, C.; Fescenko, I.; Ambal, K.; Liou, S.-H.; Lai, R. Y.; Laraoui, A. Nitrogen-Vacancy Magnetic Relaxometry of Nanoclustered Cytochrome C Proteins. *Nano Lett.* **2024**, *24*, 873−880.
(30) Wang, H.; Zhang, S.; McLaughlin, N. J.; Flebus, B.; Huang, M.; Xiao, Y.; Liu, C.; Wu, M.; Fullerton, E. E.; Tserkovnyak, Y.; et al. Noninvasive measurements of spin transport properties of an antiferromagnetic insulator. *Science Advances* **2022**, *8*, eabg8562.
(31) de Guillebon, T.; Vindolet, B.; Roch, J.-F.; Jacques, V.; Rondin, L. Temperature dependence of the longitudinal spin relaxation time T 1 of single nitrogen-vacancy centers in nanodiamonds. *Phys. Rev. B* **2020**, *102*, 165427.
(32) Khoo, J. Y.; Pientka, F.; Lee, P. A.; Villadiego, I. S. Probing the quantum noise of the spinon Fermi surface with NV centers. *Phys. Rev. B* **2022**, *106*, 115108.
(33) Ma, T.; Wang, S. *Phase transition dynamics*; Springer, 2014.
(34) Jin, C.; Tao, Z.; Kang, K.; Watanabe, K.; Taniguchi, T.; Mak, K. F.; Shan, J. Imaging and control of critical fluctuations in two-dimensional magnets. *Nat. Mater.* **2020**, *19*, 1290−1294.
(35) Jarmola, A.; Acosta, V.; Jensen, K.; Chemerisov, S.; Budker, D. Temperature-and magnetic-field-dependent longitudinal spin relaxation in nitrogen-vacancy ensembles in diamond. *Phys. Rev. Lett.* **2012**, *108*, 197601.
(36) Mrózek, M.; Rudnicki, D.; Kehayias, P.; Jarmola, A.; Budker, D.; Gawlik, W. Longitudinal spin relaxation in nitrogen-vacancy ensembles in diamond. *EPJ. Quantum Technology* **2015**, *2*, 1−11.

https://doi.org/10.1021/acs.nanolett.4c05401
Nano Lett. 2025, 25, 1473−1479